Stress–strain in electron-beam activated polymeric micro-actuators

Davide Giambastiani, Fabio Dispinzeri, Francesco Colangelo, Stiven Forti, Camilla Coletti, Alessandro Tredicucci, Alessandro Pitanti, and Stefano Roddaro

View Online   Export Citation   CrossMark

ARTICLES YOU MAY BE INTERESTED IN

Stress–strain in electron-beam activated polymeric micro-actuators

Davide Giambastiani,[1,2,a)] Fabio Dispinzeri,[1,2] Francesco Colangelo,[2,b)] Stiven Forti,[3] Camilla Coletti,[3,4] Alessandro Tredicucci,[1,2] Alessandro Pitanti,[2,c)] and Stefano Roddaro[1,2]

AFFILIATIONS

[1]Dipartimento di Fisica "E. Fermi," Università di Pisa, Largo B. Pontecorvo 3, I-56127 Pisa, Italy
[2]NEST, CNR—Istituto Nanoscienze and Scuola Normale Superiore, piazza San Silvestro 12, I-56127 Pisa, Italy
[3]Center for Nanotechnology Innovation @NEST, Istituto Italiano di Tecnologia, Piazza San Silvestro 12, I-56127 Pisa, Italy
[4]Graphene Labs, Istituto Italiano di Tecnologia, Via Morego 30, I-16163 Genova, Italy

[a)]**Author to whom correspondence should be addressed:** davide.giambastiani@phd.unipi.it
[b)]**Permanent address:** Institute for Quantum Electronics, ETH Zürich, CH-8093 Zürich, Switzerland.
[c)]**Electronic mail:** alessandro.pitanti@nano.cnr.it

ABSTRACT

Actuation of thin polymeric films via electron irradiation is a promising avenue to realize devices based on strain engineered two-dimensional materials. Complex strain profiles demand a deep understanding of the mechanics of the polymeric layer under electron irradiation; in this article, we report a detailed investigation on electron-induced stress on a poly-methyl-methacrylate (PMMA) thin film material. After an assessment of stress values using a method based on dielectric cantilevers, we directly investigate the lateral shrinkage of PMMA patterns on epitaxial graphene, which reveals a universal behavior, independent of the electron acceleration energy. By knowing the stress–strain curve, we finally estimate an effective Young's modulus of PMMA on top of graphene, which is a relevant parameter for PMMA-based electron-beam lithography and strain engineering applications.

I. INTRODUCTION

The mechanical deformation of polymers under electrostatic forces, electrostriction, ion insertion, and molecular conformation changes is a well known effect and can be exploited for creating polymeric artificial muscles.[1] Recently, this concept has been shifted to nanoscale actuators, and few experiments have demonstrated that two-dimensional (2D) materials can be strained by simply releasing part of a stressed poly-methyl-methacrylate (PMMA) layer[2] or by acting on specific regions of the polymer using a focused electron beam (e-beam). In particular, e-beam induced polymerization of a spin-on-glass material[3] and the shrinkage of PMMA[4,5] under large dose irradiation have been successfully used to control the local strain of graphene and other 2D materials. This latter technique offers a key advantage: the deformation of the target layer can be controlled with great freedom by defining a custom e-beam pattern and thus by controlling the local stress induced in the PMMA actuator. Moreover, the spontaneous

or heat-induced mechanical relaxation of the polymer over time allows us to apply different strain profiles to the same device, in a sequence of actuation-relaxation cycles.[4] This is at odds with other techniques based on e-beam irradiation of metallic layers such as Ni,[3] which instead gives permanent strain profiles.

In a more standard context, the mechanical deformation of resists during lithographic exposure has been widely studied in the literature, with the aim of improving the resolution and precision of the features of the polymeric masks. A number of possible deformation mechanisms have been identified and investigated, including the thermal annealing of the resist due to electron irradiation;[6,7] the evaporation of trapped solvents;[8] and chemical reactions leading to chain scission and recombination during irradiation.[9–12] Given the qualitatively different target of these studies, the polymeric layer typically displays a strong adhesion to the substrate, which is not ideal for the calibration of the large lateral deformations in our polymeric actuators. In addition, the

investigation of resist thinning[6,9,12]—although surely useful for lithography—does not allow a reliable quantification of isotropic stress, which is a critical parameter to accurately design and predict the strain configuration induced by a planar actuator on a 2D material.

In this article, we quantitatively investigate the mechanical properties of PMMA resist under electron exposure. First, we calibrate the PMMA stress from the mechanical response of PMMA/Si$_3$N$_4$ cantilevers after irradiation. We also independently perform a quantitative estimation of the in-plane deformation of a PMMA layer using a low-friction substrate consisting of epitaxial bilayer graphene (BLG) on SiC. Based on these experiments, we fully characterize the mechanical response of our actuators and we derive a PMMA effective Young's modulus of 1.7 ± 0.1 GPa, which is comparable with the values reported in the literature.[13–15] Our calibration is relevant not only for applications of polymer-based strain engineering but also for any device whose behavior is affected by stress transfer at the interface between a polymeric layer and a 2D material.[16–18] Applications go from the use of cross-linked PMMA as an anchorage for mechanical resonators[19] or for composite graphene/PMMA suspended membranes[20] up to stretchable/wearable devices,[21–23] where the shear forces and sliding between a 2D material and its soft substrate are particularly relevant.

II. RESULTS AND DISCUSSION

A. Stress–dose calibration with cantilevers

The measurement of the deformation of a cantilever due to a thin overlayer is a well established method to measure the internal stresses stored in the coating material during the deposition process[24–26] or during thermal expansion.[27,28] By taking advantage of this technique, we measure the stress of a thin PMMA film as a function of the e-beam exposure parameters. The cantilevers are fabricated in an array of fourfold sets, with a fixed width of $20\,\mu$m and lengths in a range from 40 to $70\,\mu$m. A typical cantilever set is shown in the SEM picture in Fig. 1(a). Spin-coating the polymeric layer on top of flexible, suspended cantilever is not an ideal method for obtaining a thin and uniform PMMA film; we resorted to a transfer technique similarly to what was routinely done with 2D materials.[29] The fabrication procedure of the Si$_3$N$_4$-cantilevers is described in detail in Appendixes A–D. Once the devices have been fabricated, the calibration procedure follows the sketch of Fig. 1(b): when the PMMA layer is exposed to e-beam radiation, the resulting rearrangement of the molecular structure and further effects tend to shift its mechanical equilibrium to a more compact configuration. This is typically modeled by introducing a "prestress" $\sigma_0 > 0$ in the constitutive relation $\sigma - \sigma_0 = C{:}\varepsilon$, where C is the stiffness tensor. In the case of the PMMA $-$ Si$_3$N$_4$ bilayer, mechanical equilibration leads to an upward bending of the cantilever. The measurement of the beam deformation by optical profilometry [see Fig. 1(c)] allows us to estimate σ_0, which is the key parameter for the design of the polymeric actuators.

Our analysis is based on the inverse bending radius of the cantilever, i.e., the curvature κ, which directly relates to σ_0. The value of κ is extracted by fitting the height profiles using a second-order polynomial.[26] However, since the cantilever is already slightly bent upward due to the non-homogeneous tensile stress in Si$_3$N$_4$ along the growth direction,[30] we also measure the initial curvature κ_0 immediately before the PMMA actuation. Subsequently, an
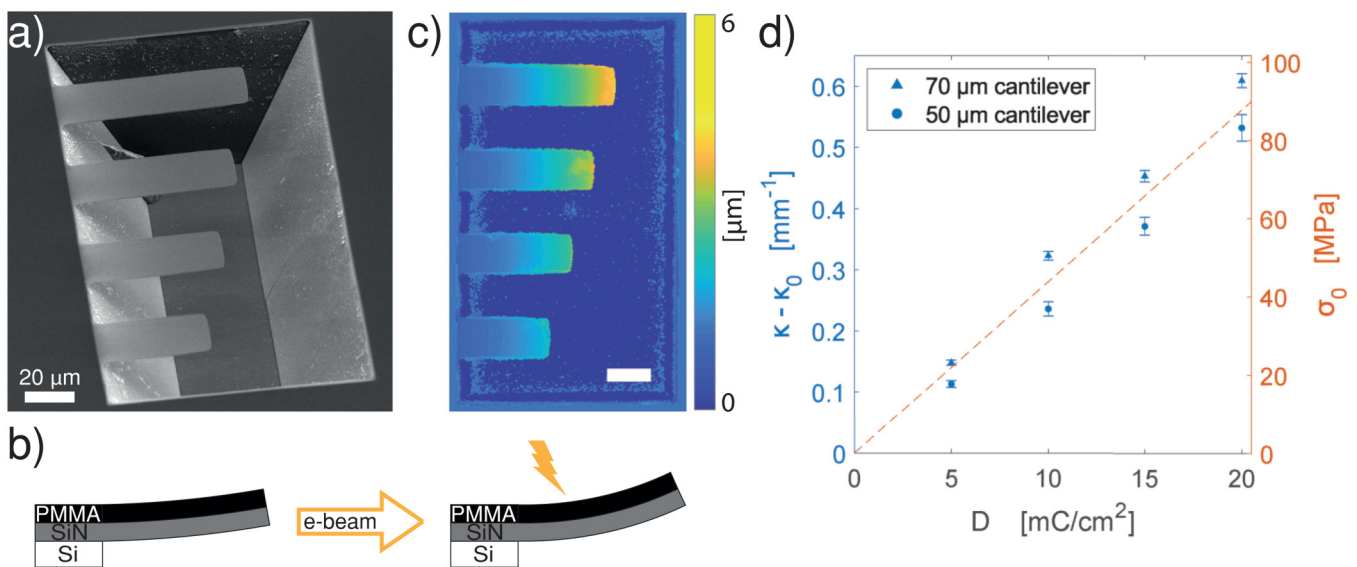
FIG. 1. (a) SEM image of the cantilevers. (b) Sketch of the actuation mechanism: the cantilever has a different curvature before (left) and after (right) e-beam irradiation. (c) A typical height map taken at the optical profilometer (scale bar is $20\,\mu$m). (d) Differential curvature $\kappa - \kappa_0$ for the $70\,\mu$m (triangles) and $50\,\mu$m (dots) cantilever as a function of the exposure doses (blue); curvature values are converted in stress values based on finite element simulations (orange dashed line, referring to the orange scale) after averaging the data for the two cantilever lengths.

additional tensile stress is applied by irradiating the PMMA with the e-beam at 5 keV. After each exposure step, we measured the 50 μm- and 70 μm-cantilever curvature κ and the resulting incremental curvature $\kappa - \kappa_0$, as reported in Fig. 1(d).

In order to convert the measured curvature values into stress, we used a finite element solver (COMSOL Multiphysics) and a cantilever model composed by two different layers with perfect adhesion (see Appendixes A–D). The bottom one is a 300 nm-thick Si_3N_4 layer with Young's modulus $E_{SiN} = 250$ GPa and Poisson ratio $\nu = 0.23$. In the case of the top PMMA layer, we carefully took into account the thinning due to the e-beam irradiation, which is known to occur at low doses.[6,9] To this end, we measured the pristine and irradiated PMMA by atomic force microscopy: the thickness of pristine PMMA was found to be 97.7 ± 1.2 nm while we measured a thickness of $49-56$ nm for the irradiated one, depending on the exact dose in the explored $5-20$ mC/cm^2 range. As argued in the following, the cantilever curvature is not particularly sensitive to the exact Young's modulus of the PMMA layer; differently, it is strongly sensitive on the value of the radiation-induced stress σ_0 of the polymeric layer. In particular, we verified that the relationship between σ_0 and κ is linear and has a very weak dependence on the PMMA Young's modulus in the range $1-10$ GPa: 10 GPa in fact led to a slope of $\kappa(\sigma_0)$ that is only 2% smaller than the one obtained for 1 GPa (for further discussion, see Appendixes A–D). This result agrees with previous numerical estimates[31] where the residual stress of a thin film deposited on a plate was calculated from the curvature of the substrate, finding a weak dependence on Young's modulus of the coating (see Sec. II C). As a result, we decided to use a standard 50 nm thickness and a PMMA Young's modulus of 1 GPa in all our simulations. The resulting conversion between curvature and stress values is visible in the right axis of Fig. 1(d), where we averaged the data measured for the 50 and 70 μm cantilevers since the simulated curvature as a function of the stress is essentially independent from the cantilever length. For the studied dose range, we observe that the estimated stress is proportional to the exposure dose D and the stress–dose data can be satisfactorily fitted by a linear function $\sigma_0 = \alpha D$ with

$$\alpha = (439 \pm 35) \, \text{N/mC}. \tag{1}$$

We note that the resulting experimental uncertainty ($\approx 6\%$) is substantially larger than the simulation error deriving from our lack of knowledge of the exact value of Young's modulus of the PMMA overlayer.

B. Strain-dose calibration on epitaxial graphene

Since the value of Young's modulus is an important parameter to predict the behavior of the actuators, we performed a complementary experiment where we estimated the PMMA lateral shrinkage as a function of e-beam energy and dose. To this end, a set of PMMA patterns were fabricated on top of epitaxial bilayer graphene (BLG) grown on SiC (0001).[32–36] The reason for this choice is twofold: (i) this experimental configuration is relevant for other strain-engineering experiments;[5] (ii) we expect a relatively small friction and thus an easy lateral shrinkage of PMMA, given the

flatness of the BLG/SiC substrate[37] and based on the results for adhesion at polymer/graphene interfaces.[16–18] The PMMA layer was spin-coated at 2000 rpm for 1 min, baked at 90 °C for 15 min, and patterned by standard e-beam lithography. The cross section of the system is sketched in Fig. 2(a). The basic experimental procedure is sketched in Fig. 2(b): in a sequence of exposure steps, we first irradiate the PMMA with the e-beam and then measure the resulting shrinkage. Since SEM imaging already leads to a well-defined exposure of the PMMA, the measurement simply consists of a continuous image scanning of the polymer. The advantage of this technique is that PMMA can be actuated and probed very quickly while keeping a steady environment, minimizing natural mechanical relaxation. The first (left) and last (right) SEM images of one of the patterned squares over the BLG/SiC substrate in a sequence of exposure steps are depicted in Fig. 2(c).

In each measurement, we estimated the contraction of PMMA along the two sides of the square based on the contrast profile in the SEM image and calculated the average planar strain $\bar{\varepsilon}$. An evident PMMA shrinkage up to about 10% is observed; the resulting trend is displayed in Fig. 3(a) as a function of electron dose D
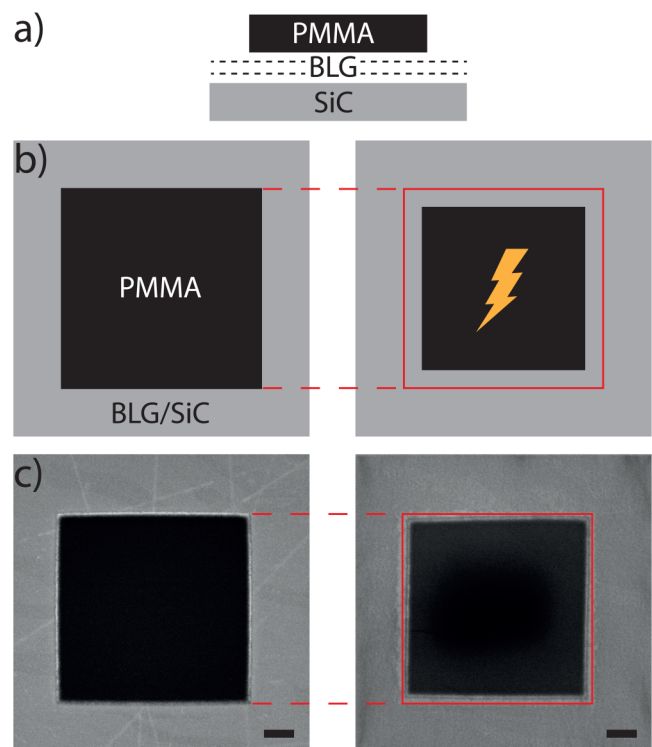
FIG. 2. (a) Schematic cross section of the device under investigation with the bilayer epitaxial graphene (BLG) grown on SiC and a patterned square of PMMA. (b) Schematic of the actuation process: on the left, the square before and, on the right, the square after the e-beam irradiation. (c) First (left) and last (right) SEM image of one of the patterned squares in a sequence of irradiation steps at 2 keV. The dark square is PMMA while the bright region is the epitaxial graphene. The black bars are 600 nm.

and at a set of different electron energies E relevant for actuators, in a range from $E = 2$ to $10\,keV$. All the curves share a qualitatively similar trend: (i) in the typical operational range of our actuators, the shrinkage initially displays a linear dependence on the dose with a slope $v = d\bar{\varepsilon}/dD$; (ii) beyond a given threshold, the shrinkage tends to saturate. Both the slope of the linear region v and the saturation threshold are found to strongly depend on the beam energy E and for every given dose, we observe a larger shrinkage at smaller energies.

A dependence of the shrinkage on the electron energy is indeed not unexpected, because the number of collisions between the electrons and the PMMA molecules depends strongly on the

beam energy. In fact, PMMA is completely opaque to electrons at low energy, while it becomes almost transparent at high energies where most of the scattering occurs in the underlying substrate. In particular, collision events are expected to decay once the penetration depth exceeds the PMMA thickness.

In order to investigate how the electron energy affects the shrinkage of the PMMA, we performed a Monte Carlo simulation of the collision of 10^4 electrons with a $50\,nm$ layer of PMMA; the estimate has been done using a freely available software.[38,39] The number of collisions $n_{coll}(E)$ has been calculated for several energies E, neglecting effects due to reflections of electrons from the substrate and secondary electron generation. The relative number of collisions $n_R = n_{coll}(E)/n_{coll}(2\,keV)$, defined using the $2\,keV$ case as a reference, is reported in Fig. 3(b) (orange line). Below $2\,keV$, the number increases with energy and reaches a maximum around $1\,keV$, while a marked decrease is observed at larger energies due to the increased penetration depth of the e-beam. A comparison between the relative number of electron–atom collisions and the observed PMMA shrinkage clearly shows that the simulated effect largely explains the energy dependence we observe in our data. This can be easily seen in Fig. 3(b): the relative slope $v_R = v(E)/v(2\,keV)$ (blue line) matches very nicely with the results of the Monte Carlo simulation (orange line). Based on this observation, we define an effective electron dose D_{eff}, again using $2\,keV$ as a reference,

$$D_{eff} = \frac{D(E) \cdot n_{coll}(E)}{n_{coll}(2\,keV)},\qquad(2)$$

and obtain that all the shrinkage-dose curves roughly collapse on a unique universal behavior, independent of the electron energy employed in the experiment (see Fig. 4). We note that the regime we investigate is different from what was reported in other lower
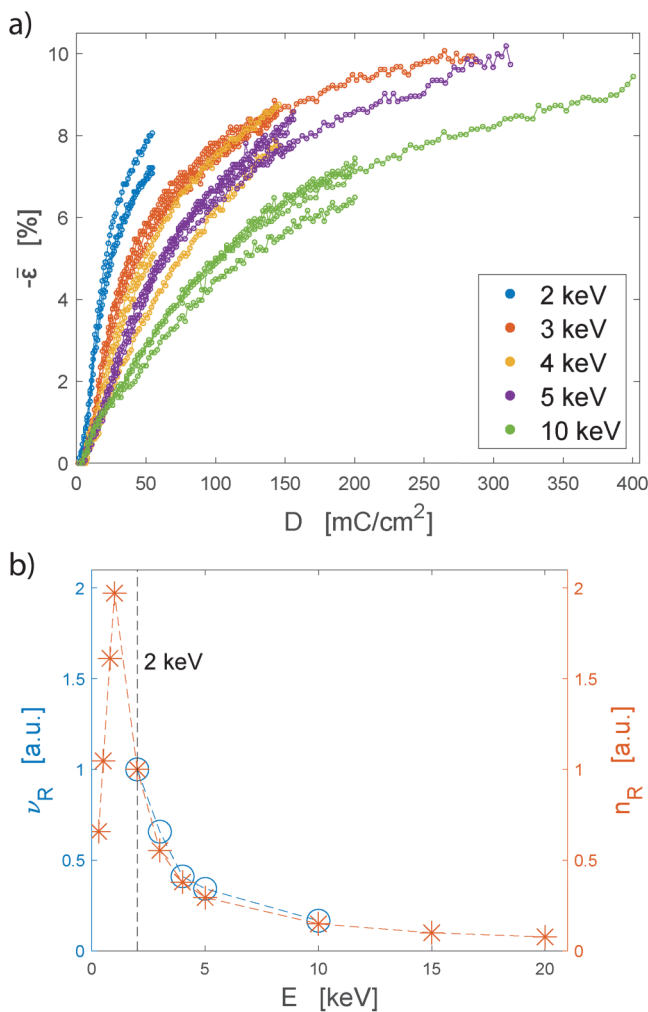
FIG. 3. (a) Measured average planar strain $\bar{\varepsilon}$ of the PMMA squares as a function of the electron dose D and beam energy E. Different curves of the same color represent different squares analyzed, at the corresponding energy. (b) Dependence of the slope, v_R, on the electron energy (blue) and simulated number of electron–atom collisions, n_R (orange).
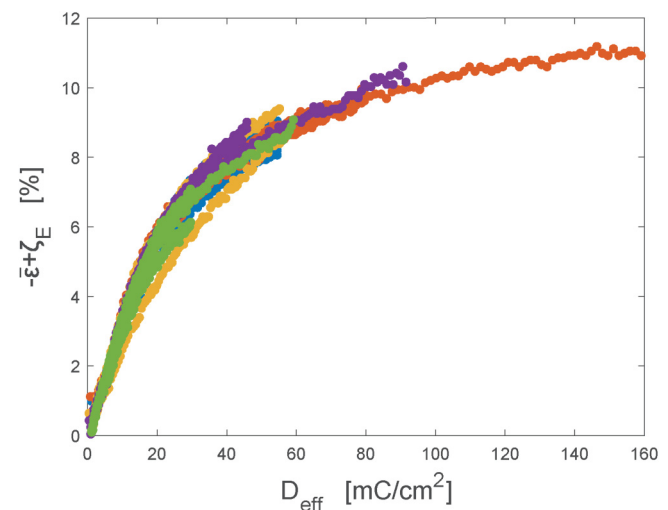

FIG. 4. Universal trend of the shrinkages, translated by ζ_E (see Appendixes A–D), as a function of the effective dose. The color code is the same as that in Fig. 3.

energy studies,[6,8,9] where the penetration depth is smaller than the PMMA thickness and larger shrinkage is observed at larger energy. This regime is not ideal for actuators since it is important to include a uniform shrinkage throughout the whole PMMA thickness; thus, the penetration depth has to be large.

One interesting aspect of our experiment consists in the relative friction between PMMA and the underlying epitaxial graphene, which we assumed here to be negligible. On the other hand, it is also known that, upon exposure, the resist can display some interlayer adhesion and be used to strain an underlying 2D material.[4,5] The exact mechanisms leading to adhesion are still under investigation, but our previous works showed that beam irradiation is a crucial factor and increases adhesion, compared to that observed for unexposed PMMA.[4] Adhesion is also likely to be promoted by a rough interface topography but, since BLG/SiC is atomically flat, such effects should be minimized in our experimental configuration.

C. Combined analysis

Results from Secs. II A and II B can be combined to extract an estimate of the expected free shrinkage of PMMA as a function of the applied stress, in the linear actuation regime. This allows assessing the mechanical properties of our PMMA. In Fig. 5, we report the data obtained by averaging the results of shrinkage experiments obtained on three different PMMA squares at 5 keV. In the plot, the dose D has been converted into a PMMA stress σ_0 based on the results of the cantilever calibration. Using the stress–strain relation for a homogeneous stress,[40] we fit the data and estimate an effective Young's modulus of 1.7 ± 0.1 GPa for the e-beam actuated PMMA. Despite the measured PMMA Young's modulus could
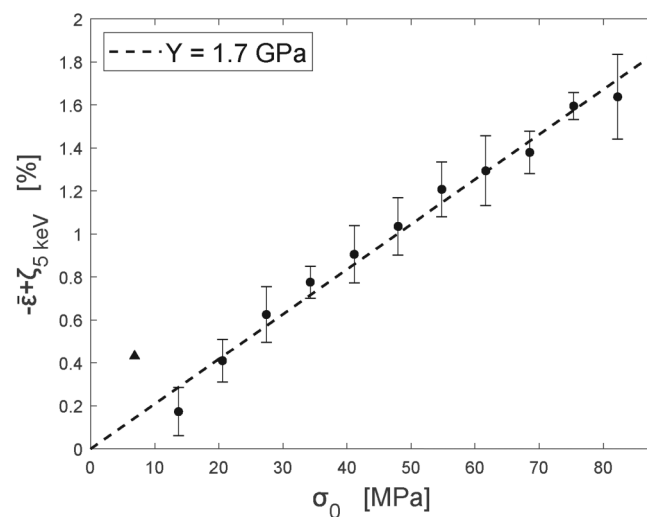
FIG. 5. Average values of the shrinkage for three different PMMA squares, at each value of dose, as a function of the simulated stress calibrated with Eq. (1). The error-bars are the standard deviation of the measured PMMA squares. The triangle is defined to be the reference value ($\bar{\varepsilon} = 0$). The dashed line is the numerical fit of data from which we estimate Young's modulus Y.

be affected by the chemical modifications and heating during e-beam exposure, the values are well within the range between 1 and 3 GPa obtained by Yamazaki *et al.*[15]

III. CONCLUSION

In conclusion, we studied the mechanical response of PMMA under e-beam irradiation to extract useful parameters for the design of PMMA-based actuators. This was accomplished using two complementary methods: in a first set of experiments, PMMA was deposited on Si_3N_4-cantilevers and the stress vs dose response was evaluated based on the mechanical deflection of the cantilever and on finite element simulations; in a second set of experiments, the free contraction of PMMA patterned onto an epitaxial BLG was investigated. Our study highlights that the strong energy dependence we observe in the mechanical response above 2 keV can be largely explained in terms of an energy-dependent number of electron collision in the PMMA. As a result, we found a universal shrinkage-dose curve that is valid in the whole energy range relevant to the actuators. Finally, from the comparison of these two results, we estimate the effective Young's modulus of PMMA patterned onto epitaxial BLG. Our work provides a benchmark for future applications of PMMA as an e-beam actuating layer for strain engineering of 2D materials and for investigating the mechanical response of other polymeric thin films.

APPENDIX A: Si_3N_4-CANTILEVER FABRICATION AND PMMA TRANSFER

The substrate consists of a 250 μm commercial silicon wafer sandwiched between two 300 nm thick stoichiometric silicon nitride layers deposited with PECVD at high temperature ($\approx 850\,°C$) in order to have a strong residual tensile stress at room temperature. For the definition of the sets of cantilevers, S1818 was spin-coated on the sample at 4000 rpm for 1 min. After 1 min of baking at 90 °C and pre-developing in MF-319 and H_2O, we patterned the sets of cantilevers through laser writer lithography exposing with a wavelength of 385 nm and energy dose of 150 mJ/cm². The sample was then baked 20 s at 120 °C and the pattern was developed in MF-319 and H_2O. The S1818 was used as a mask for CF_4-based plasma etching. Then, wet etching of Si (KOH:H_2O 30% at 70 °C) was performed. The resulting trench in the Si substrate is designed to be deep enough so that the device can survive wet processing and the resulting capillarity forces, which are relevant during the drying phase.

The preparation of PMMA (AR-P 679.02) for the transfer consisted of spin-coating in two successive steps, polyvinyl alcohol and PMMA, both at 2000 rpm for 1 min and baked at 90 °C for

1 min, on silicon. Finally, the PMMA was removed from the substrate placing the sample in H_2O at $90\,°C$ and was transferred onto the cantilevers and baked at $110\,°C$ for 1 min. The suspended PMMA was patterned by e-beam lithography and developed in a solution of methyl isobutyl ketone and isopropyl alcohol (1:3) for 2 min and rinsed in isopropyl alcohol in order to remove the portions of PMMA outside the cantilevers. In order to avoid charging effects, a conductive layer (ESPACER) is also used to coat the devices before the actuation experiment.

The profiles of the cantilevers were taken before and after electron irradiation at 5 keV, using a commercial optical profilometer (Taylor-Hobson, CCI HD).

APPENDIX B: ANALYSIS OF THE SEM PROFILES

The size of the PMMA squares is measured extracting the profiles from each SEM image (1200×1200 pixels), which extends over an area of $6 \times 6\,\mu m$. In order to reduce the noise, we performed an average of contiguous line-profiles corresponding to $0.4\,\mu m$ and calculated the vertical and horizontal size of the PMMA square. From the analysis, we found that the vertical size of the PMMA is slightly larger than the horizontal one. The initial discrepancy of about 2.9% tends to decrease during e-beam irradiation and reaches about 2.5% at large electron doses. Regarding the analysis of the shrinkage during e-beam irradiation, we found that the first exposure apparently expands the PMMA ($\bar{\varepsilon} > 0$). This effect is visible only for energies smaller than 10 keV and is probably due to charging of PMMA. In order to correct this systematic effect, we fitted the linear trend at low-doses (for each energy) with

$$-\bar{\varepsilon} = v \cdot D - \zeta, \tag{B1}$$

where v is defined in Sec. II B and ζ is the offset.

APPENDIX C: FINITE ELEMENT SIMULATIONS

The Stoney formula[41,42] gives the curvature $\tilde{\kappa}$ of a plate as a function of the planar stress of a thin deposited film σ_f,

$$\sigma_f = \frac{t_s^2 Y_s}{6 t_f (1 - v_s)} \tilde{\kappa}, \tag{C1}$$

where t, Y, and v are thickness, Young's modulus, and Poisson's ratio of the substrate (indicated with the subscript s) and the thin film (subscript f), respectively. If the thin film thickness is comparable to the substrate one, the formula can be corrected with an extra term, which depends linearly on the ratio between the two thicknesses t_f/t_s,[31]

$$\sigma_f = \frac{t_s^2 Y_s}{6 t_f (1 - v_s)} \tilde{\kappa} \times \left[1 + \left(4 \frac{Y_f (1 - v_s)}{Y_s (1 - v_f)} - 1 \right) \frac{t_f}{t_s} \right]. \tag{C2}$$

Even if Stoney's formula was obtained for unclamped plates, as a first Approximation, it can be used to describe the curvature of clamped cantilevers. Therefore, we compared the analytical results of Eq. (C2) with finite element simulations of an initially flat

PMMA/Si_3N_4 cantilever subjected to a planar stress of the PMMA layer. We found a good agreement between analytical results and simulations, with a maximum discrepancy of the ratio $\tilde{\kappa}/\sigma_f$ of about 9%, considering Young's modulus of PMMA Y_f in a range from 1 to 10 GPa. Also, as previously discussed, Eq. (C2) shows a weak dependence from Y_f, with a few percent difference when the two extremal values in the considered range are used. The comparison between Eq. (C2) (which successfully reproduced numerical results[31]) and our numerical simulations of flat cantilevers, validates our model, enabling its use for more complex geometries (prebended cantilevers), as the ones investigated in our experiment.

As mentioned in Sec. II A, we stress that a fundamental assumption of the model is that the two layers in the beam display a perfect adhesion. This means that the two materials are stuck together with no inter-layer sliding between each other. In fact, no measurable shrinkage of PMMA could be observed in e-beam experiments performed on SiC or on Si_3N_4 at odds with the experiments on BLG/SiC reported in the main text.

APPENDIX D: EPITAXIAL GRAPHENE ON SILICON CARBIDE

Epitaxial BLG was grown starting from nominally on-axis Si-face polished 6H-SiC(0001) purchased from SiCrystal Gmb. The synthesis of BLG was carried out by thermal decomposition, adapting the recipe of Emtsev and co-workers[32] in an Aixtron Black Magic reaction chamber, using an Ar backpressure of 780 mbar and a sublimation temperature of $1395\,°C$, measured with a single-wavelength infrared pyrometer focused on the sample.

DATA AVAILABILITY

The data that support the findings of this study are available from the corresponding author upon reasonable request.

REFERENCES

[1]T. Mirfakhrai, J. D. Madden, and R. H. Baughman, "Polymer artificial muscles," Mater. Today **10**, 30–38 (2007).

[2]I. Polyzos, M. Bianchi, L. Rizzi, E. N. Koukaras, J. Parthenios, K. Papagelis, R. Sordan, and C. Galiotis, "Suspended monolayer graphene under true uniaxial deformation," Nanoscale **7**, 13033–13042 (2015).

[3]H. Shioya, M. F. Craciun, S. Russo, M. Yamamoto, and S. Tarucha, "Straining graphene using thin film shrinkage methods," Nano Lett. **14**, 1158–1163 (2014).

[4]F. Colangelo, A. Pitanti, V. Mišeikis, C. Coletti, P. Pingue, D. Pisignano, F. Beltram, A. Tredicucci, and S. Roddaro, "Controlling local deformation in graphene using micrometric polymeric actuators," 2D Mater. **5**, 045032 (2018).

[5]F. Colangelo, A. Morandi, S. Forti, F. Fabbri, C. Coletti, F. V. Di Girolamo, A. Di Lieto, M. Tonelli, A. Tredicucci, A. Pitanti et al., "Local tuning of WS2 photoluminescence using polymeric micro-actuators in a monolithic van der Waals heterostructure," Appl. Phys. Lett. **115**, 183101 (2019).

[6]A. Habermas, D. Hong, M. F. Ross, and W. R. Livesay, "193-nm CD shrinkage under SEM: Modeling the mechanism," in Metrology, Inspection, and Process Control for Microlithography XVI (International Society for Optics and Photonics, 2002), Vol. 4689, pp. 92–101.

[7]G. Ayal, D. Andelman, and Y. Cohen, "Analytical model for ARF photoresist shrinkage under scanning electron microscopy inspection," J. Vac. Sci. Technol. B **27**, 1976–1983 (2009).

[8]T. Kudo, J.-B. Bae, R. R. Dammel, W.-K. Kim, D. S. McKenzie, M. D. Rahman, M. Padmanaban, and W. Ng, "CD changes of 193-nm resists during SEM

measurement," in *Advances in Resist Technology and Processing XVIII* (International Society for Optics and Photonics, 2001), Vol. 4345, pp. 179–189.

[9]T. Sarubbi, M. F. Ross, M. Neisser, T. Kocab, B. T. Beauchemin Jr., W. R. Livesay, S. S. Wong, and W. Ng, "Mechanism studies of scanning electron microscope measurement effects on 193-nm photoresists and the development of improved line-width measurement methods," in *Advances in Resist Technology and Processing XVIII* (International Society for Optics and Photonics, 2001), Vol. 4345, pp. 211–221.

[10]T. Azuma, K. Chiba, H. Abe, H. Motoki, and N. Sasaki, "Mechanism of ARF resist-pattern shrinkage in critical-dimension scanning electron microscopy measurement," J. Vac. Sci. Technol. B **22**, 226–230 (2004).

[11]B. Bunday, A. Cordes, J. Allgair, V. Tileli, Y. Avitan, R. Peltinov, M. Bar-zvi, O. Adan, E. Cottrell, and S. Hand, "Phenomenology of electron-beam-induced photoresist shrinkage trends," in *Metrology, Inspection, and Process Control for Microlithography XXIII* (International Society for Optics and Photonics, 2009), Vol. 7272, p. 72721B.

[12]M. Yasuda, Y. Furukawa, H. Kawata, and Y. Hirai, "Multiscale simulation of resist pattern shrinkage during scanning electron microscope observations," J. Vac. Sci. Technol. B **33**, 06FH02 (2015).

[13]B. Briscoe, L. Fiori, and E. Pelillo, "Nano-indentation of polymeric surfaces," J. Phys. D Appl. Phys. **31**, 2395 (1998).

[14]C. M. Stafford, C. Harrison, K. L. Beers, A. Karim, E. J. Amis, M. R. VanLandingham, H.-C. Kim, W. Volksen, R. D. Miller, and E. E. Simonyi, "A buckling-based metrology for measuring the elastic moduli of polymeric thin films," Nat. Mater. **3**, 545–550 (2004).

[15]K. Yamazaki, T. Yamaguchi, and H. Yamaguchi, "Modulation of Young's modulus of poly (methyl methacrylate) nanobeam due to electron-beam exposure," Jpn. J. Appl. Phys. **46**, L1225 (2007).

[16]L. Gong, I. A. Kinloch, R. J. Young, I. Riaz, R. Jalil, and K. S. Novoselov, "Interfacial stress transfer in a graphene monolayer nanocomposite," Adv. Mater. **22**, 2694–2697 (2010).

[17]T. Jiang, R. Huang, and Y. Zhu, "Interfacial sliding and buckling of monolayer graphene on a stretchable substrate," Adv. Funct. Mater. **24**, 396–402 (2014).

[18]G. Anagnostopoulos, C. Androulidakis, E. N. Koukaras, G. Tsoukleri, I. Polyzos, J. Parthenios, K. Papagelis, and C. Galiotis, "Stress transfer mechanisms at the submicron level for graphene/polymer systems," ACS Appl. Mater. Interfaces **7**, 4216–4223 (2015).

[19]P. Weber, J. Guttinger, I. Tsioutsios, D. E. Chang, and A. Bachtold, "Coupling graphene mechanical resonators to superconducting microwave cavities," Nano Lett. **14**, 2854–2860 (2014).

[20]J. Xu, G. Wood, A. Al-mashaal, E. Mastropaolo, M. Newton, and R. Cheung, "Realization of closed cavity resonator formed by graphene-PMMA membrane for sensing audio frequency," IEEE Sens. J. **20**, 4618–4627 (2020).

[21]D. Akinwande, N. Petrone, and J. Hone, "Two-dimensional flexible nanoelectronics," Nat. Commun. **5**, 1–12 (2014).

[22]H. Jang, Y. J. Park, X. Chen, T. Das, M.-S. Kim, and J.-H. Ahn, "Graphene-based flexible and stretchable electronics," Adv. Mater. **28**, 4184–4202 (2016).

[23]H. Jang, Z. Dai, K.-H. Ha, S. K. Ameri, and N. Lu, "Stretchability of PMMA-supported CVD graphene and of its electrical contacts," 2D Mater. **7**, 014003 (2019).

[24]S. Johansson, F. Ericson, and J.-Å. Schweitz, "Influence of surface coatings on elasticity, residual stresses, and fracture properties of silicon microelements," J. Appl. Phys. **65**, 122–128 (1989).

[25]H. Ljungcrantz, L. Hultman, J.-E. Sundgren, S. Johansson, N. Kristensen, J.-Å. Schweitz, and C. Shute, "Residual stresses and fracture properties of magnetron sputtered Ti films on Si microelements," J. Vac. Sci. Technol. A **11**, 543–553 (1993).

[26]W. Fang and J. Wickert, "Comments on measuring thin-film stresses using bi-layer micromachined beams," J. Micromech. Microeng. **5**, 276 (1995).

[27]W.-H. Chu, M. Mehregany, and R. L. Mullen, "Analysis of tip deflection and force of a bimetallic cantilever microactuator," J. Micromech. Microeng. **3**, 4 (1993).

[28]W. Fang, H.-C. Tsai, and C.-Y. Lo, "Determining thermal expansion coefficients of thin films using micromachined cantilevers," Sens. Actuators A **77**, 21–27 (1999).

[29]H. Van Ngoc, Y. Qian, S. K. Han, and D. J. Kang, "PMMA-etching-free transfer of wafer-scale chemical vapor deposition two-dimensional atomic crystal by a water soluble polyvinyl alcohol polymer method," Sci. Rep. **6**, 33096 (2016).

[30]W. Shi, H. Zhang, G. Zhang, and Z. Li, "Modifying residual stress and stress gradient in LPCVD Si_3N_4 film with ion implantation," Sen. Actuators A **130–131**, 352–357 (2006).

[31]A. Mézin, "Coating internal stress measurement through the curvature method: A geometry-based criterion delimiting the relevance of Stoney's formula," Surf. Coat. Technol. **200**, 5259–5267 (2006).

[32]K. V. Emtsev, A. Bostwick, K. Horn, J. Jobst, G. L. Kellogg, L. Ley, J. L. McChesney, T. Ohta, S. A. Reshanov, J. Röhrl *et al.*, "Towards wafer-size graphene layers by atmospheric pressure graphitization of silicon carbide," Nat. Mater. **8**, 203–207 (2009).

[33]C. Riedl, U. Starke, J. Bernhardt, M. Franke, and K. Heinz, "Structural properties of the graphene-SiC(0001) interface as a key for the preparation of homogeneous large-terrace graphene surfaces," Phys. Rev. B **76**, 245406 (2007).

[34]K. Emtsev, F. Speck, T. Seyller, L. Ley, and J. Riley, "Interaction, growth, and ordering of epitaxial graphene on SiC(0001) surfaces: A comparative photoelectron spectroscopy study)," Phys. Rev. B **77**, 155303 (2008).

[35]S. Goler, C. Coletti, V. Piazza, P. Pingue, F. Colangelo, V. Pellegrini, K. V. Emtsev, S. Forti, U. Starke, F. Beltram *et al.*, Revealing the atomic structure of the buffer layer between SiC(0001) and epitaxial graphene," Carbon **51**, 249–254 (2013).

[36]S. Forti and U. Starke, "Epitaxial graphene on SiC: From carrier density engineering to quasi-free standing graphene by atomic intercalation," J. Phys. D Appl. Phys. **47**, 094013 (2014).

[37]P. N. First, W. A. de Heer, T. Seyller, C. Berger, J. A. Stroscio, and J.-S. Moon, "Epitaxial graphenes on silicon carbide," MRS Bull. **35**, 296–305 (2010).

[38]D. Drouin, A. R. Couture, D. Joly, X. Tastet, V. Aimez, and R. Gauvin, "CASINO v2.42—A fast and easy-to-use modeling tool for scanning electron microscopy and microanalysis users," Scanning **29**, 92–101 (2007).

[39]H. Demers, N. Poirier-Demers, A. R. Couture, D. Joly, M. Guilmain, N. de Jonge, and D. Drouin, "Three-dimensional electron microscopy simulation with the casino Monte Carlo software," Scanning **33**, 135–146 (2011).

[40]L. D. Landau and E. Lifshitz, *Course of Theoretical Physics, Theory of Elasticity* (Elsevier, 1986), Vol. 7.

[41]G. G. Stoney, "The tension of metallic films deposited by electrolysis," Proc. R. Soc. London Ser. A **82**, 172–175 (1909).

[42]G. C. Janssen, M. M. Abdalla, F. Van Keulen, B. R. Pujada, and B. Van Venrooy, "Celebrating the 100th anniversary of the Stoney equation for film stress: Developments from polycrystalline steel strips to single crystal silicon wafers," Thin Solid Films **517**, 1858–1867 (2009).